Bull Volcanol (2009) 71:79–94
DOI 10.1007/s00445-008-0210-5

RESEARCH ARTICLE

The occurrence of Mt Barca flank eruption in the evolution of the NW periphery of Etna volcano (Italy)

S. Branca · P. Del Carlo · M. D. Lo Castro · E. De Beni · J. Wijbrans

Received: 14 July 2007 / Accepted: 4 March 2008 / Published online: 8 April 2008

Abstract Geological surveys, tephrostratigraphic study, and $^{40}Ar/^{39}Ar$ age determinations have allowed us to chronologically constrain the geological evolution of the lower NW flank of Etna volcano and to reconstruct the eruptive style of the Mt Barca flank eruption. This peripheral sector of the Mt Etna edifice, corresponding to the upper Simeto valley, was invaded by the Ellittico volcano lava flows between 41 and 29 ka ago when the Mt Barca eruption occurred. The vent of this flank eruption is located at about 15 km away from the summit craters, close to the town of Bronte. The Mt Barca eruption was characterized by a vigorous explosive activity that produced pyroclastic deposits dispersed eastward and minor effusive activity with the emission of a 1.1-km-long lava flow. Explosive activity was characterized by a phreatomagmatic phase followed by a magmatic one. The geological setting of this peripheral sector of the volcano favors the interaction between the rising magma and the shallow groundwater hosted in the volcanic pile resting on the impermeable sedimentary basement. This process produced phreatomagmatic activity in the first phase of the eruption, forming a pyroclastic fall deposit made of high-density, poorly vesicular scoria lapilli and lithic clasts. Conversely, during the second phase, a typical strombolian fall deposit formed. In terms of hazard assessment, the possible occurrence of this type of highly explosive flank eruption, at lower elevation in the densely inhabited areas, increases the volcanic risk in the Etnean region and widens the already known hazard scenario.

Keywords Etna volcano · Unconformity · Tephrostratigraphy · $^{40}Ar/^{39}Ar$ age determination · Flank eruption · Eruptive style · Simeto River

Editorial responsibility: R Cioni

S. Branca (✉) · P. Del Carlo · M. D. Lo Castro · E. De Beni
Istituto Nazionale di Geofisica e Vulcanologia,
Sezione di Catania,
Piazza Roma 2,
95123 Catania, Italy
e-mail: branca@ct.ingv.it

P. Del Carlo
Istituto Nazionale di Geofisica e Vulcanologia, Sezione di Pisa,
via della Faggiola 32,
56126 Pisa, Italy

J. Wijbrans
Faculteit Aard-en Levenswetenschappen, Vrije Universiteit,
Amsterdam, The Netherlands

Introduction

The eruptive history of Etna volcano during the past 60 ka has been characterized by the stabilization of the plumbing system allowing the growth of a main polygenetic eruptive center, the so-called Ellittico volcano, that forms the bulk of the present edifice (Branca et al. 2004a). In particular, during this time span, the eruptive activity of Ellittico volcano produced the expansion of the lava flows northward and westward causing a radical modification of the hydrographic network of the Simeto and Alcantara paleovalleys (Chester and Duncan 1979, 1982; Branca and Ferrara 2001; Branca 2003). In the past 15 ka, the Ellittico products were almost completely covered by the lava flows erupted during the Mongibello volcano activity fed by the same plumbing system (Branca et al. 2004a), issued by vents widely distributed on the volcano slopes along three main weakness zones, the so-called NE, S, and W rifts (Chester et al. 1985; McGuire and Pullen 1989). Ellittico and Mongibello flank eruptions are mainly effusive,

forming wide compound lava flow fields as evidenced by the analysis of the historical eruptive activity of the past three centuries (class A eruption of Branca and Del Carlo 2005). Furthermore, the authors distinguished a second type of flank eruption (class B), characterized by effusive activity associated with vigorous explosive activity at the vents lasting for most of the eruption. In particular, the explosive activity produced eruptive plumes and ash fall within tens to hundreds of kilometers from the vent. During the past three centuries, only seven class B eruptions have occurred, mostly in the nineteenth century, producing intense long-lasting explosive activity with tephra fallout. Such explosive activity related to flank eruptions was directly monitored during the 2001 and 2002–2003 eruptions. During these recent flank eruptions, lava fountain activity formed some kilometers of high volcanic plumes that fed continuous tephra fallout during most of the eruption and caused damage to the Catania and Reggio Calabria infrastructure, including the airports, and gravely impacted both the economy and health of the Etna region (Andronico et al. 2005; Scollo et al. 2007).

Recent detailed stratigraphic investigations have revealed that also the pre-historic explosive activity related to flank eruptions was complex and variable as well, showing phreatomagmatic features and forming medial–distal tephra deposits similar to those of the 2001 and 2002–2003 eruptions. In particular, on the lower north-eastern slope of Etna edifice at about 500 m elevation, a phreatomagmatic flank eruption occurred 18.7±0.1 ka BP during Ellittico volcano activity producing pyroclastic fall and surge deposits (Andronico et al. 2001). These explosive features of a flank eruption are closely related to the subsurface contact between the volcanic strata and the underlying, impermeable sedimentary basement that allowed the formation of shallow groundwater. In fact, the interaction between the feeder dike and the external water hosted in the volcanic pile resulted in phreatomagmatic instead of the more common strombolian-type activity (Andronico et al. 2001). In terms of hazard assessment, the occurrence of such explosive flank eruptions at lower altitude increases the volcanic risk in the Etnean region, extending the presently defined hazard scenario.

In this framework, we have studied the Mt Barca flank eruption located in the western periphery of Etna edifice close to the town of Bronte at about 15.5 km away from the summit craters (Fig. 1). A new 1:10,000 scale geological mapping was carried out on the lower western flank of the volcano along the left bank of the Simeto River. Geological data presented in this paper are based on unconformity-bounded units (Salvador 1987, 1994), adopted to draw up the new geological map of Etna (Branca et al. 2004b). Furthermore, we have performed a tephrostratigraphic study of the pyroclastic succession of the Mt Barca eruption together with petro-chemical analyses of the volcanics. We also present the results of new $^{40}Ar/^{39}Ar$ age determinations. This isotopic technique was applied successfully on Etna volcano (De Beni et al. 2005; Branca et al. 2008) with the aim of chronologically constraining the new stratigraphic setting proposed by Branca et al. (2004a).

The whole data set allows us to chronological define the geological evolution of this poorly investigated peripheral sector of the Etna volcano and to reconstruct the eruptive style of the Mt Barca eruption in order to provide further information on this type of explosive flank eruptions.

Geological setting and volcanological evolution of Mount Etna volcano

Mount Etna volcano is located between the Gela-Catania Foredeep and the frontal nappes of the Appenninic-Maghrebian Orogen (Fig. 1) related to the Neogene convergence between Africa and Europe plates (Lentini 1982; Ben Avraham and Grasso 1990).

Volcanism at Mount Etna is divided into four phases according to Branca et al. (2004a, 2008). The oldest phase, named Basal Tholeiitic, corresponds to a long period of discontinuous and scattered eruptive activity, which began about 500 ka ago within the Gela-Catania Foredeep basin through fissure-type submarine eruptions. This phase ended about 300 ka ago with fissure-type eruptions in a sub-aerial environment, forming a wide lava plateau developed on the

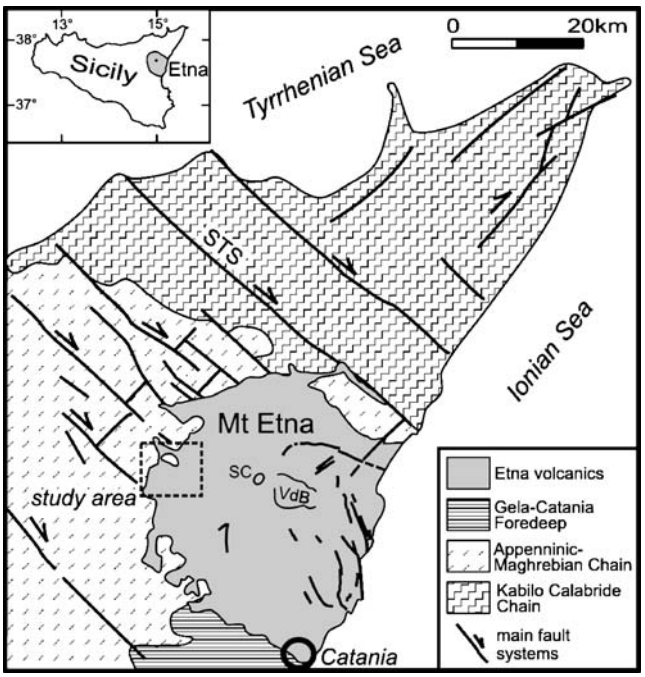

Fig. 1 Geological and structural sketch map of Sicily (modified after Branca et al. 2008). *SC* Summit craters, *VdB* Valle del Bove, *STS* South Tyrrhenian system

old alluvial plain of the paleo-Simeto River. Between 220 and 121 ka ago, the Timpe phase volcanism was mainly concentrated along the Ionian coast building a primitive shield volcano. In this time span, scattered effusive eruptions also took place in a wide area corresponding to the present lower SW and SE flanks of Etna. Furthermore, the eruptive activity shifted westward at the end of this phase, for the first time, toward the central region of the volcano corresponding to the present day Val Calanna area. During the third phase, named Valle del Bove Centers, the stabilization of the magma source in the Valle del Bove area and the beginning of the central-type volcanism occurred with the formation of several small polygenic volcanic centers. In particular, the early edifices recognized are represented by the Tarderia and Rocche volcanoes whose activity ended between 106 and 102 ka ago. Thereafter, the volcanism was mainly concentrated on the southwestern side of the Valle del Bove with the formation of the Trifoglietto volcano and other minor eruptive centers. Finally, the Stratovolcano phase combines the products of the Ellittico and Mongibello volcanoes. Ellittico volcanic activity started at about 60 ka and ended 15 ka ago with four caldera-forming plinian eruptions (Coltelli et al. 2000). During the post-15 ka, persistent basaltic volcanic activity formed the Mongibello volcano through summit and flank eruptions whose products cover about 85% of Etna's surface.

Stratigraphy of lower NW flank

In the study area, the sedimentary basement of the volcano is formed by the Sicilide Complex units of the Appenninic-Maghrebian Chain (Fig. 2), comprising the tectonic units of the Numidian Flysch (Upper Oligocene–Lower Miocene) and of the Varicolored Clays (Cretaceous–Eocene; Lentini et al. 2006).

These sedimentary terrains are partially covered by the lava flows of the Stratovolcano phase that crop out along the left bank of the Simeto River valley. In particular, the Ellittico volcano products consist of five superimposed porphyritic lava flow fields (E1, E2, E3, E4, and E5 in Fig. 2) along the valley floor that are separated by thin paleosol, epiclastic, and alluvial deposits as subsurface data evidenced (Fig. 3). The oldest E1 is a massive lava, about 20 m thick, showing well-developed columnar jointing with

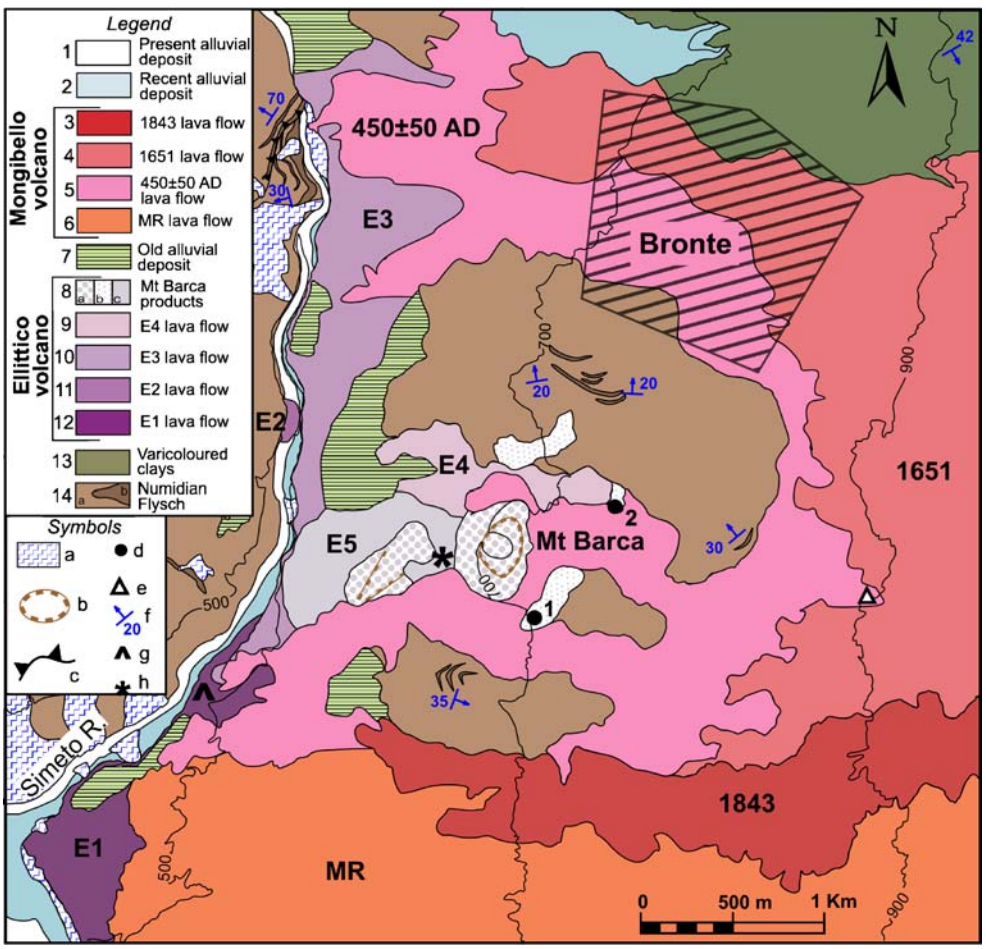

Fig. 2 Geological map of the lower NW flank of Etna. Legend: *1* Present alluvial deposit; *2* recent alluvial deposit; *3* 1843 lava flow; *4* 1651 lava flow; *5* 450±50 AD lava flow; *6* MR lava flow; *7* old alluvial deposit; *8* Mt Barca products: *a* scoria cone, *b* pyroclastic deposit, *c* E5 lava flow; *9* E4 lava flow; *10* E3 lava flow; *11* E2 lava flow; *12* E1 lava flow; *13* varicolored clays; *14* Numidian Flysch: *a* brown clays and *b* quartz-arenites. Symbols: *a* landslides; *b* crater rim; *c* thrust fault; *d* Contrada Ciapparo (*1*) and Contrada Contura (*2*) sections; *e* bore hole; *f* strata attitude; *g* BT sample (coordinate 37°46′10″ N–14°48′16″ E); *h* MC sample (coordinate 37°46′26″ N–14°49′10″ E)

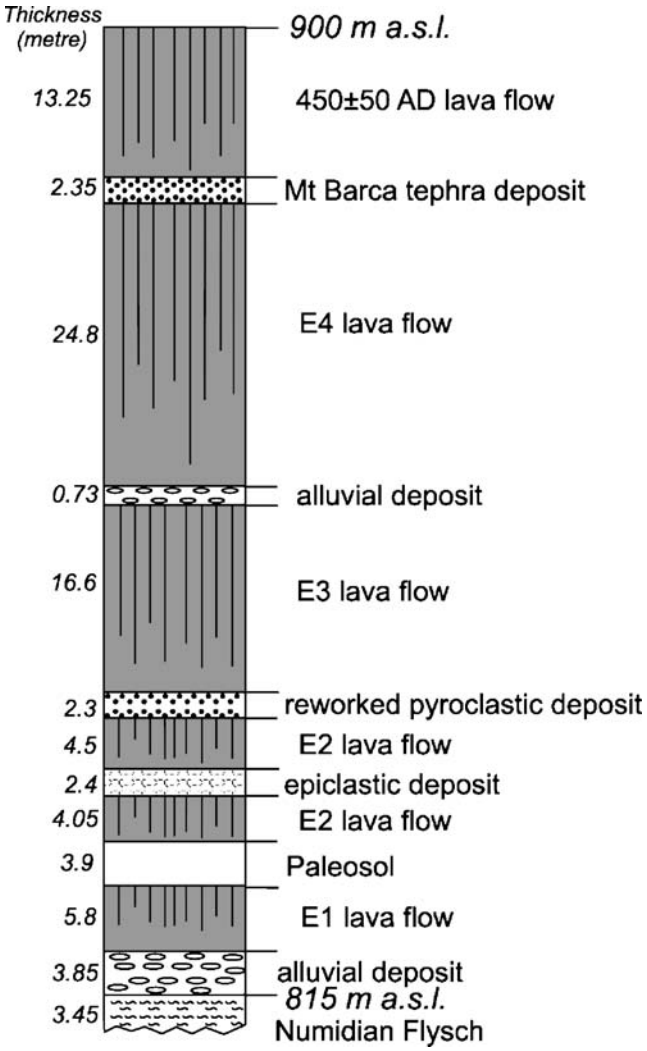

Fig. 3 Stratigraphy of the borehole located at Contrada Ciapparazzi. For location, see Fig. 2

prevalent toothpaste morphology (Rowland and Walker 1987). E2 lava flow consists of highly porphyritic lava with abundant plagioclase phenocrysts, up to 8 mm in size, forming a small outcrop about 5 m thick. E3 lava flow is a massive lava, about 25 m thick characterized by well-developed columnar jointing that overlays the previous E1 and E2 lava flows. E4 is a thin lava flow forming a restricted outcrop located between Mt Barca and the sedimentary terrains. Finally, E5 is a lava flow, at least 1.1 km long, originated by the Mt Barca eruptive fissure that is located between 580 and 700 m elevation close to the town of Bronte (Fig. 2). The eruptive fissure is marked by the large scoria cone of Mt Barca and by a spatter rampart, elongated NE–SW, made up of welded scoriaceous bombs. Furthermore, pyroclastic deposits of Mt Barca scoria cone discontinuously crop out immediately north and east of the eruptive fissure (Fig. 2). Overall, the E1, E3, and E5 lava flows form a terraced body along the left bank of the Simeto River as a consequence of the erosional processes connected to the entrenchment of the drainage patterns. This morphogenetic process produced an alluvial deposit, 4–6 m thick, made up of sand and clay with sandstone pebbles partially covering the Ellittico lava flow fields (Fig. 2).

The products of the Mongibello volcano consist of one pre-historic porphyritic lava flow field (MR in Fig. 2) characterized by an "aa" morphology that covered both the sedimentary basement and the E1 lava flow. In particular, the MR lava flow field is generated by the large Mt Ruvolo scoria cone located at 1,400 m elevation on the W rift out of the study area. Subsequent products of Mongibello activity comprise a historical lava flow field dated 450±50 AD by Tanguy et al. (2007), that partially covered the Ellittico lava flows. Finally, the frontal portions of the 1651 and 1843 lava flow fields represent the most recent products that have reached this peripheral sector of the volcano.

In addition to surface data, an 88-m-deep geognostic continuous coring down to the sedimentary basement has allowed the reconstruction of the subsurface stratigraphy (Fig. 3). In particular, the geognostic coring was performed at 900 m elevation about 2 km eastward of Mt Barca scoria cone (Sturiale 1967). The sedimentary basement was found at 815 m elevation and is made up of brown clay of the Numidian Flysch. The top of the volcanic succession is formed by the 450±50 AD lava flow showing a thickness of 13.25 m (Fig. 3). The main portion of the succession comprises all the Ellittico products cropping out in the study area represented by Mt Barca, 2.35-m-thick, pyroclastic fall deposit, and by the E4, E3, E2, and E1 lava flows (Fig. 3). Thin alluvial, epiclastic, and reworked pyroclastic deposits are interlayered within the Ellittico lava succession.

Description of Mt Barca eruption deposits

Mt Barca scoria cone

The Mt Barca eruption was characterized by vigorous explosive activity that produced widespread pyroclastic deposits and minor effusive activity. Along the eruptive fissure, which is partially covered by the historical lava flow of 450±50 AD, Mt Barca scoria cone shows an asymmetrical morphology with an elliptical shape, a low height/basal diameter ratio (0.19), and a maximum height of 747 m a.s.l. The cone is formed by an alternation of welded scoriaceous weathered lapilli and bread crust bombs layers. About 200 m west of the cone is a spatter rampart, NE–SW-elongated, made of pinkish-altered scorias with a plagioclase-rich nucleus. A lava flow was generated from the base of the scoria cone (E5 in Fig. 2) partially overlying the spatter rampart deposit.

Tephrostratigraphy

Mt Barca fallout deposits have mainly been found E of the cone. In particular, at Contrada Ciapparo and Contrada Contura, about 300 m SE and 600 m NE respectively, two outcrops show a complex pyroclastic succession several meters thick (Fig. 2). Northward, poorly preserved fallout tephra deposits have been found overlaying the Flysch Numidian clays. The Contrada Ciapparo and Contrada Contura stratigraphic sections have been studied in detail, tephra layers have been measured and described, and 19 samples collected for laboratory analyses.

Contrada Ciapparo section

The Contrada Ciapparo section is a ca. 6-m-thick tephra succession; the basal contact on the sedimentary substratum is not visible (Fig. 4). The lowermost deposit is a 96-cm-thick, poorly sorted layer, mostly made of angular centimeter-sized lithic clasts and coarse dense lapilli, showing a faint stratification. Lithics are quartzarenitic clasts, clay blocks, quartz fragments, and monolithologic lava clasts. A sharp contact separates this deposit from the overlaying succession formed by an alternation of black scoriaceous lapilli and ash beds. These deposits are characterized by the presence of thin, yellowish, and hardened ash horizons containing fine lapilli covered by a yellowish patina, found at different heights along the section. Finally, dispersed juvenile ballistic bombs are present.

Contrada Contura section

Contrada Contura section is a 7-m-thick compound section resulting from the stratigraphic correlation of two very close outcrops (Fig. 5). As in the Contrada Ciapparo section, the base of the tephra succession is not visible. Deposits show similar features to those of the previous section, as the presence of lithic clasts and the yellowish-hardened ash beds in the lowermost part. The lowermost deposits consist of a gray lithic-rich ash layer followed by a 5–6-cm-thick horizon made of black sub-rounded fine scoria lapilli. Afterwards, a 4–7-cm-thick, gray tuff bed overlies a 71-cm-thick black scoria lapilli and lithic fragments layer. This deposit is topped by a 30-cm-thick coarse scoria lapilli layer containing bread crust bombs and coarse lithic clasts. Following this, a ca. 80-cm-thick black scoria lapilli presents at the top and at the base two tuff beds. The section continues with an alternation of ash beds with stratified scoria and lithic lapilli layers followed by a 30-cm-thick-stratified plane-parallel deposit made up of laminated ash tuff beds, 2–3 cm thick, alternated with rounded fine lapilli horizons, about 4 cm thick, containing reddish lithic fragments. The upper part of the section is characterized by a 76-cm-thick highly vesicular, black scoria lapilli with two thin, yellowish-hardened ash horizons and fine lapilli covered by a yellowish patina at the base, the same as we found in the Contrada Ciapparo section. Lithic fragments have the same nature of those found in the Contrada Ciapparo section. The Contrada Contura section is topped by a 1-m-thick reworked deposit made of volcanogenic material followed by a reddish paleosol overlain by the Roman age lava flow (Fig. 5).

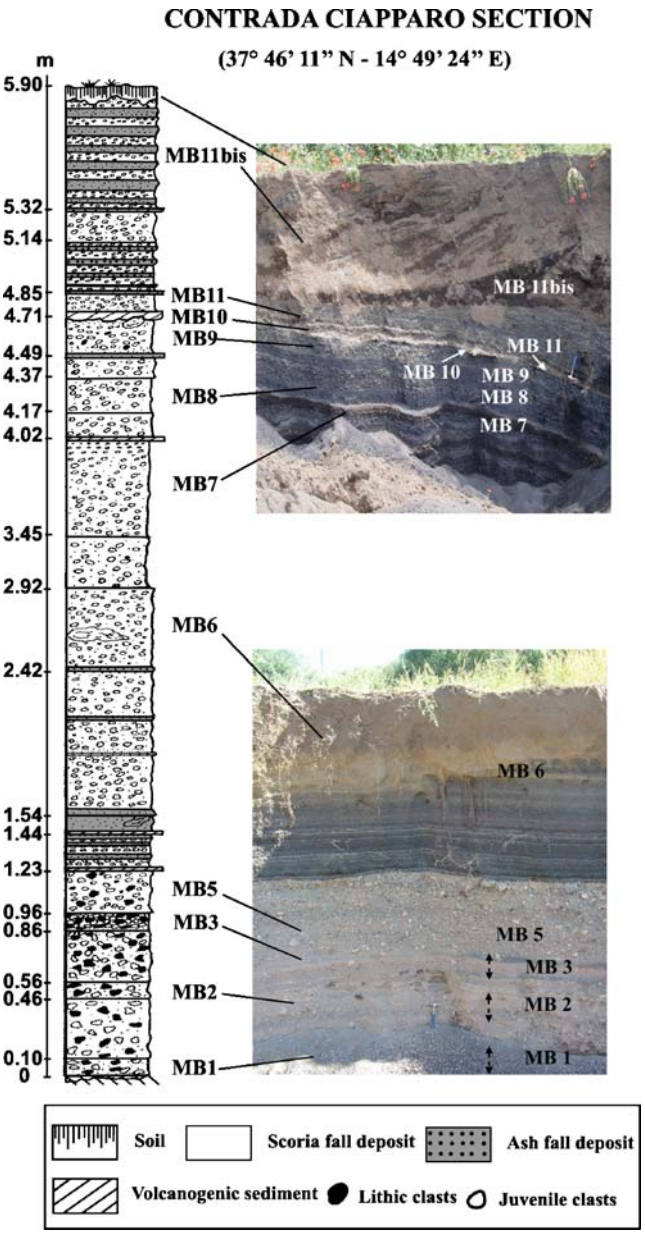

Fig. 4 Stratigraphy of Contrada Ciapparo section. The labels from MB1 to MB11bis indicate samples locations for laboratory analysis. For location of the section, see Fig. 2

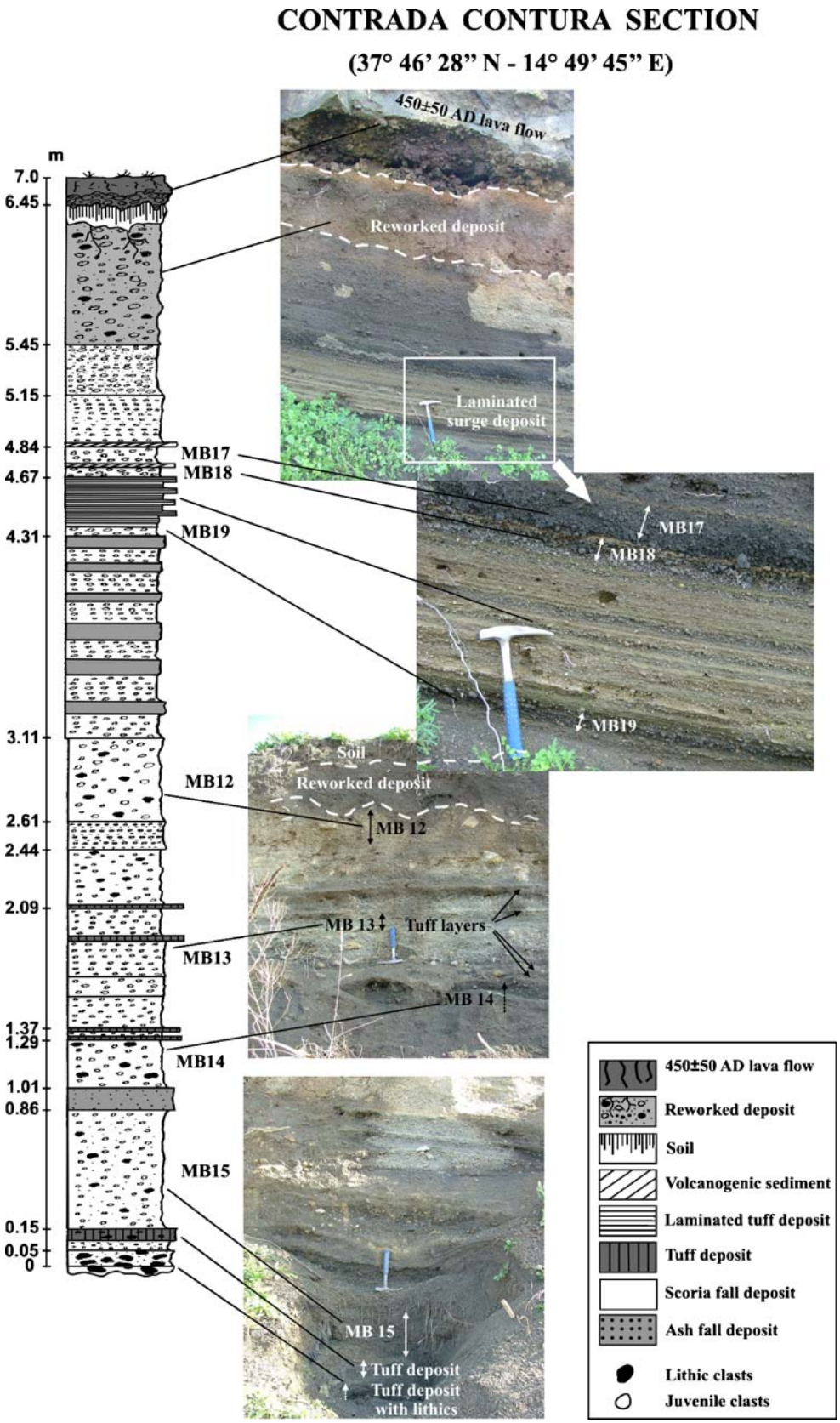

Fig. 5 Stratigraphy of Contrada Contura section. The labels from MB12 to MB19 indicate the locations of the samples for laboratory analysis. For location of the section, see Fig. 2

Analytical data

Methods

In order to determine the physical characteristic of Mt Barca deposits, 18 samples (from MB1 to MB19 in Figs. 4 and 5) were collected for grain-size, componentry, density, and petro-chemical analyses that were performed at the Istituto Nazionale di Geofisica e Vulcanologia, Sezione di Catania laboratories. One-phi interval grain-size analyses of tephra were done by dry sieving in a range between 0.032 and 32 mm, and component analysis was carried out in order to distinguish juvenile from lithic fraction, by hand picking, in the class 32–1-mm interval and by means of observations at the microscope. Density analyses were performed on 30 juvenile clasts per sample in the class of 8 mm, with a Mohr-Westphal precision balance based on the water displacement method. To avoid water adsorption, juvenile clasts were coated with an impermeable film. Petrographic characteristics have been determined by optical microscope observations on thin sections, including Mt Barca lava flow, spatter rampart scorias, and tephra. Bulk rock analyses of one lava flow sample and three pyroclasts have been performed by Activation Laboratories Ltd. (Canada) to measure the composition of the major elements. Scanning electron microscopy analyses were performed on two scoria samples in order to determine glass composition. Measurements have been done with a LEO-1430 scanning electron microscope equipped with an Oxford EDS micro-analytical system (SEM–EDS). Analytical conditions are 20 keV of acceleration tension, 1,200 nA of beam current, and XPP data reduction routine. To minimize sodium loss during analysis, a square raster of 10 μm was used. Replicate analyses of the international standard VG-2 Glass basaltic (Jarosewich et al. 1980) were performed as analytical control. The precision expressed as relative standard deviation is less than 1% for SiO_2, Al_2O_3, FeOtot, and CaO and less than 3% for TiO_2, MnO, Na_2O, K_2O, and P_2O_5.

Results

Grain-size histograms of the studied samples show a unimodal trend, with the exception of MB10 that presents a bimodal pattern (Figs. 6 and 7). In both sections, the basal deposits are characterized by a coarser grain size, especially MB1, MB2, and MB3 samples from the Contrada Ciapparo section, which have a mode value of −3 phi. Median diameter and sorting parameters have been calculated from the cumulative curves and have been plotted in the classification diagram (Fig. 8; Walker 1973). This diagram illustrates that all the analyzed samples are within the field of the pyroclastic fall deposits, excluding the MB10 sample that falls in the pyroclastic flow deposits field. Nevertheless, the stratigraphic features of this layer, such the constant thickness along the outcrop, the wide dispersal area with decreasing thickness with the distance from the vent, indicate a more likely pyroclastic fall origin of this layer. Its grain-size parameters are related to a poor sorting of the deposit caused by the presence of scoria lapilli entrapped within the ash bed from the underlying deposit.

Component analysis shows that lithic fragments of sedimentary type consist of the Numidian Flysch quartz-arenitics, whereas lava clasts belong to the E4 lava flow. Juvenile typology varies from highly vesiculated with irregular morphology to poorly vesiculated and dense, with a blocky and rounded morphology. The maximum percentage of lithic fraction is relative to MB1, MB2, and MB3 samples belonging to the basal deposits of Contrada Ciapparo section with a maximum value of 32 wt.% in the MB3 sample. In this section, from MB5 to MB11bis samples the lithic percentage drops radically to zero in the uppermost layers. On the contrary, in the Contrada Contura section, there is a smaller amount of lithic clasts reaching a maximum value of 13% in the MB14 sample. Nevertheless, the lithic fraction is present in all this section, except for the topmost level relative to the MB17 sample.

As far as the density analysis of juvenile clasts is concerned, the MB1, MB2, and MB3 samples from the basal deposits of the Contrada Ciapparo section show the highest values in a fairly narrow range between 12 and 20×10^2 kg/m^3 (Fig. 6). The other values of density in this section are comprised in a wider range between 8 and 24×10^2 kg/m^3, although the peaks are toward lower values. In the Contrada Contura section, density values are similar to those of the Contrada Ciapparo section ($11–24\times10^2$ kg/m^3) and concentrated all over the section (Fig. 7), with a drastic decrease in the MB17 top sample that has a mean density of 11×10^2 kg/m^3 (Fig. 7), typical of well vesicular clasts formed during strombolian activity. In summary, high lithic percentage and high-density juvenile clasts characterize the basal deposits of the two sections (as far as MB5 in the Contrada Ciapparo section and the MB18 sample in the Contrada Contura, respectively), whereas the topmost levels are formed by low-density-vesiculated juvenile clasts without lithic fragments.

We carried out petrographic analyses on 11 thin sections of scoria lapilli and two of lava (Table 1). All samples have the same mineral assemblage, namely a porphyritic structure with phenocrysts of plagioclase as the most abundant phase, minor clinopyroxene and olivine that can slightly vary in their relative abundance within the sequence, and oxides. The groundmass shows the same mineral assemblage including brown glass in some scoria samples from the strombolian deposits. Lava (C8, MC) and spatter rampart (DS) samples have a higher porphyritic index (P.

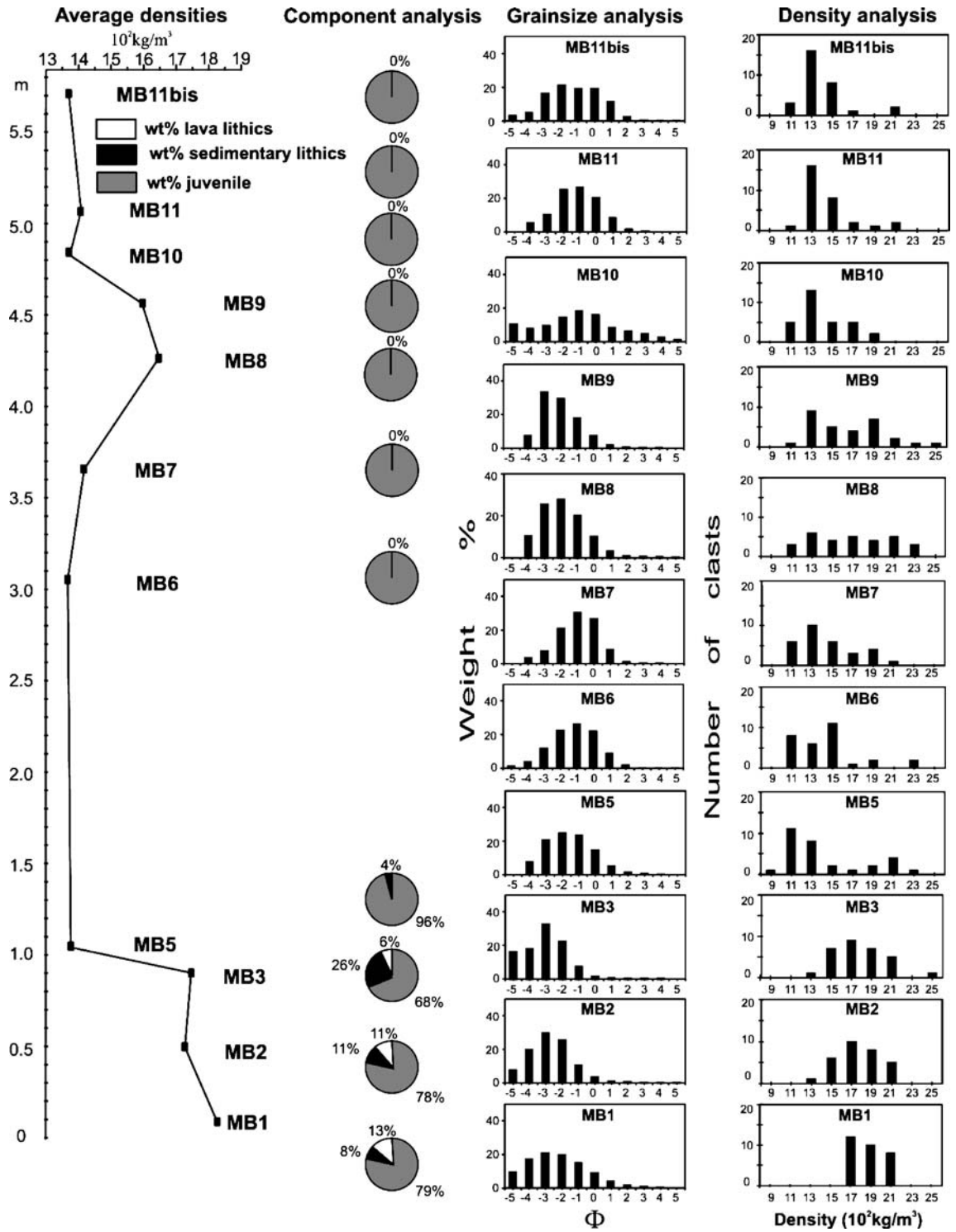

Fig. 6 Component, grain-size, and density analyses of the Contrada Ciapparo section

I.) than scoria lapilli showing larger phenocrysts of plagioclase. Samples from the basal deposits (MB1, MB5 and MB15, MB17) are microvesicular with a low P.I. index and contain many quartz xenocrysts belonging to the sedimentary basement, some of them partially reabsorbed, whereas the scoria lapilli of the upper levels present large coalescent bubbles and do not contain xenocrysts.

Mt Barca volcanics are hawaiite according to the total alkali silica (TAS) classification (Fig. 9; Le Maitre 1989). Glass composition was determined in two scoria samples,

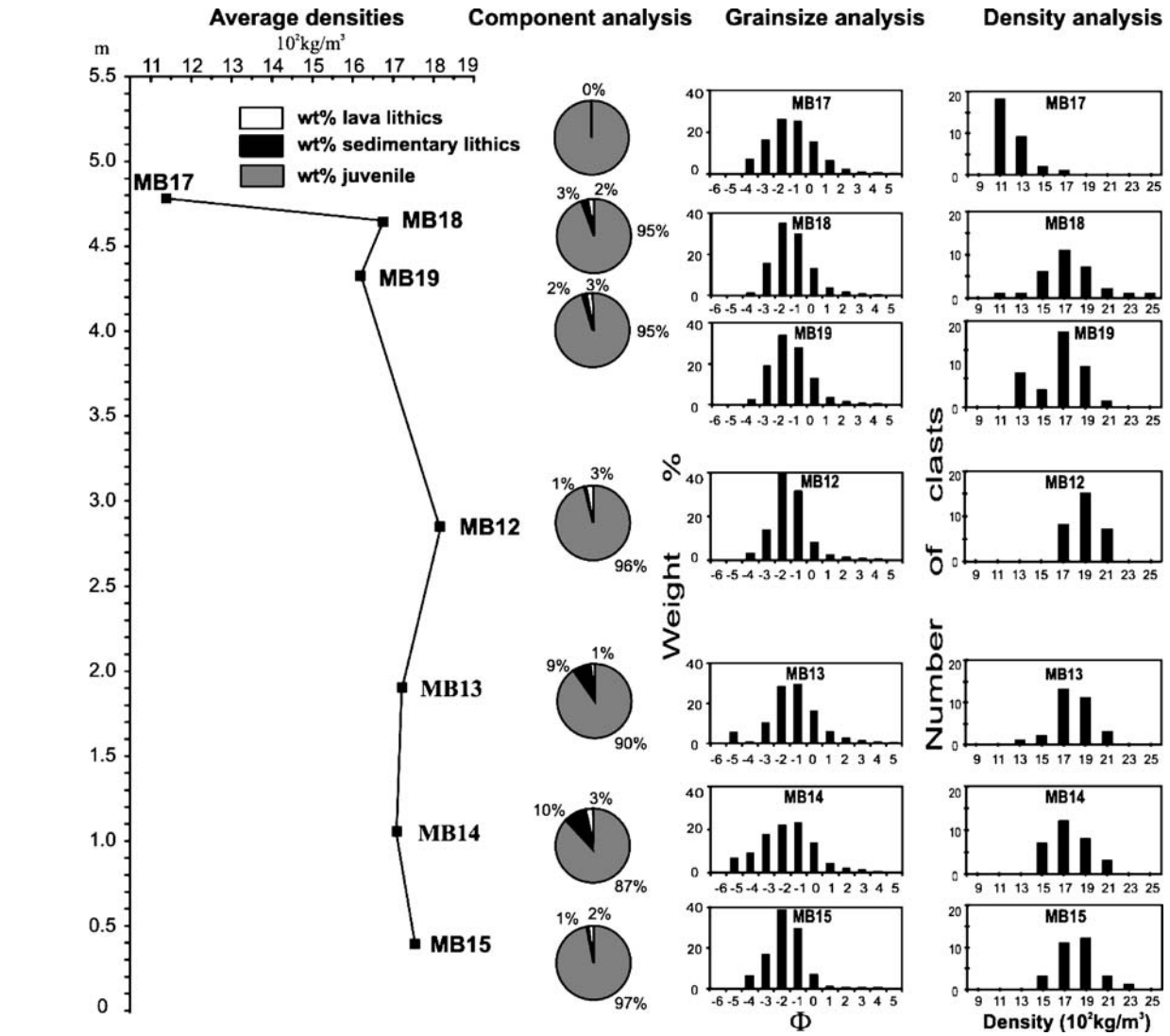

Fig. 7 Component, grain-size, and density analysis of the Contrada Contura section

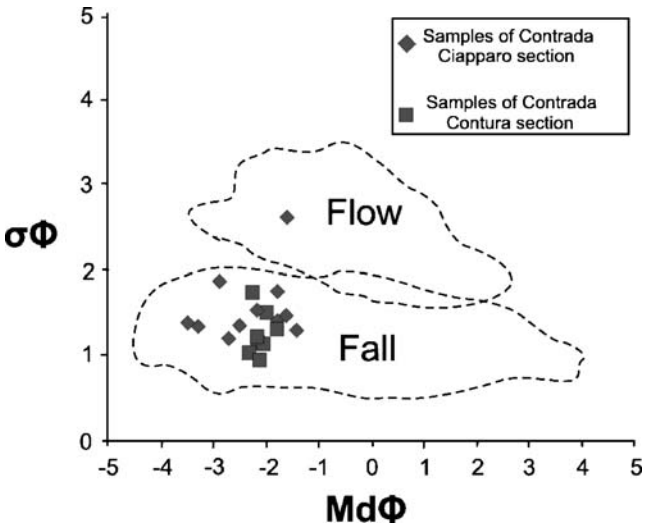

Fig. 8 Classification diagram of the pyroclastic deposits (Walker 1973); median diameter Mdϕ (=ϕ50) versus graphical standard deviation $\sigma\phi$ (=ϕ84–ϕ16/2)

MB5 (Contrada Ciapparo) and MB17 (Contrada Contura), where we found glassy areas in the groundmass to measure. They fall within the mugearitic compositional field with a silica content ranging from 52 to 54 wt.% and alkali from 6 to 7.8 wt.%. Bulk rock and glass analyses are reported in Tables 2 and 3, respectively. Bulk rock and glass compositions fall within the compositional field known for Etna volcanics erupted in the Stratovolcano phase (Corsaro and Pompilio 2004; see Fig. 9) to which Mt Barca activity belongs.

Facies analysis and analytical data allow us to stratigraphically correlate the Contrada Ciapparo and Contrada Contura sections identifying two main lithostratigraphic units, Units 1 and 2 (Fig. 10). The basal Unit 1 is characterized by a lithic-rich coarse dense scoria fall deposit, whereas Unit 2 consists of a strombolian-type pyroclastic fall deposit with no lithic clasts. The passage between the two units is very sharp in the Contrada

Table 1 Petrographic description of the Mt Barca volcanics

Sample	Rock texture	P.I. (%)	Phenocrysts assemblage	Xenocrysts	V %	Groundmass texture
C8 lava	Porphyritic	35	pl, ol, cpx, ox		–	Intergranular
MC lava	Porphyritic	35	pl, ol, cpx, ox		–	Intergranular
DS scoria	Porphyritic	30	pl, ol, cpx, ox		20	Intersertal
MB1 scoria	Porphyritic	15	pl, ol, cpx, ox	Quartzarenite	30	Intersertal
MB3 scoria	Porphyritic	20	pl, ol, cpx, ox	Quartzarenite	20	Intersertal
MB5 scoria	Porphyritic	10	pl, ol, cpx, ox		30	Intersertal
MB6 scoria	Porphyritic	10	pl, ol, cpx, ox		35	Intersertal
MB11 scoria	Porphyritic	20	pl, ol, cpx, ox		20	Intersertal
MB12 scoria	Weakly porphyritic	5	pl, ol, cpx, ox		20	Intersertal
MB13 scoria	Weakly porphyritic	3	pl, cpx, ol, ox		20	Intersertal
MB15 scoria	Weakly porphyritic	3	pl, cpx, ol, ox	Quartzarenite	30	Intersertal
MB17 scoria	Weakly porphyritic	5	pl, ol, cpx, ox	Quartzarenite	40	Intersertal
MB18 scoria	Porphyritic	5–10	pl, ol, cpx, ox		25	Intersertal

DS scoria Spatter rampart sample, *P.I.* porphyritic index, *pl* plagioclase, *ol* olivine, *cpx* clinopyroxene, *ox* oxides, *V* vesicularity

Ciapparo section with a clear separation surface between basal lithic-rich products and upper strombolian one, whereas in the Contrada Contura the passage is marked by the presence of a stratified plane-parallel deposit formed by an alternation of fine-laminated tuff beds and rounded fine lapilli horizons showing typically surge-like facies (Figs. 5 and 10).

$^{40}Ar/^{39}Ar$ data

In this paragraph, we present the results of two samples analyzed with the $^{40}Ar/^{39}Ar$ incremental heating technique, and for information on the methodological approach, see Appendix.

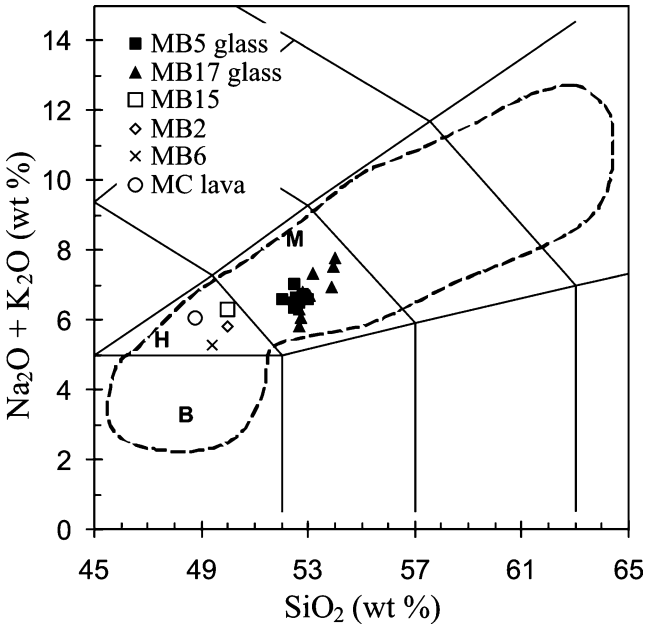

Fig. 9 Total alkali silica (TAS) diagram (Le Maitre 1989) of Mt Barca volcanics. *B* basalt, *H* hawaiite, *M* mugearite. *Dashed line* bounds the compositional field known for volcanics erupted in the last 60 ka during the Stratovolcano phase of Etna eruptive activity (from Corsaro and Pompilio 2004)

The MC sample was analyzed with nine steps of incremental heating starting from 750°C to 1,300°C. For age calculation, the last step was excluded because it does not belong to the plateau; the plateau is based on 98.5% of the total gas release (Fig. 11). The weighted plateau age is 28.7±6.3 ka (error in 1σ) with a percentage error around 22%, which is a good uncertain margin if we consider the very young age of the sample; mean-squared-weighted deviations (MSWD) value is also very low 0.27, indicating that the analytical uncertainty dominates the quoted uncertainty (e.g., Dunai and Wijbrans 2000). The K/Ca diagram shows a regular pattern of continuously decreasing ratios from 1.3 in the first step to 0.01 at fusion temperature. The total fusion age and isochrons (normal and inverse) ages are perfectly in agreement with the weighted plateau age, and the non-radiogenic intercept of the isochron $^{40}Ar/^{36}Ar$ intercept is 295.2±2.0 which is indistinguishable from that of atmospheric argon (295.5).

The BT sample was also analyzed with nine steps of incremental heating starting from 700°C to 1,250°C (Fig. 11); the number of steps and the temperature interval were chosen to obtain the most homogenous plateau that is possible. The first step was skipped from the age calculation because it does not contain a significant amount of argon; the percentage of $^{39}Ar_{(K\ derived)}$ used for the calculation is 97.8%. The weighted plateau age is 40.9± 7.2 ka (error in 1σ) with a percentage error around 17%, and MSWD is 0.03. The K/Ca diagram shows an irregular pattern characterized by a low value for the first step (0.17) then an increase for the second (0.34) and third (0.31) steps and another low value (0.22) at the fourth step; the fifth, sixth, and seventh steps are around 0.3 and with the K/Ca ratio decreasing to 0.02 in the last two steps. This behavior suggests that K-rich components in the groundmass release

Table 2 Major elements of Mt Barca volcanics

	Sample			
	MB2	MB6	MB15	MC
SiO_2	50.01	49.43	50.61	48.76
TiO_2	1.51	1.45	1.71	1.65
Al_2O_3	19.38	20.5	17.74	17.21
Fe_2O_3	9.19	8.86	10.29	10.56
MnO	0.16	0.15	0.18	0.18
MgO	3.56	3.39	4.01	5.01
CaO	8.87	9.71	8.02	9.41
Na_2O	4.30	3.98	4.61	4.24
K_2O	1.51	1.29	1.68	1.84
P_2O_5	0.75	0.70	0.84	0.81
Total	99.55	99.98	99.77	99.79

gas during steps 1, 3, 8, and 9, while Ca-rich phases (andesine and labradorite) dominate steps 2, 3, 5, 6, and 7 of the experiment. Weighted plateau and isochrons (normal and inverse) ages are perfectly in agreement and the non-radiogenic $^{40}Ar/^{36}Ar$ intercept is 296.2±5.6 within the uncertainty equal to that of air argon. In both samples, $^{38}Ar_{(Cl\ derived)}$ is generally very low (0.02 MC sample and 0.0001 BT sample); thus, we do not expect a significant interference of $^{36}Ar_{Cl}$ on the determination of radiogenic argon ($^{40}Ar^*$).

Discussion

The new geological data of the lower north-west flank of Etna volcano have revealed the presence of a main unconformity that characterizes the volcanic succession of this peripheral sector. On the whole, the periphery of the volcano edifice is characterized by variable entrenchment of drainage systems (Branca and Catalano 2000). This phenomenon produces the development of different erosional surfaces that correspond to a re-organization of the volcano periphery morphology, conditioning lava flow emplacement. In particular, the unconformity of the lower north-west flank is related to an erosional phase marked by the entrenchment of the paleo-Simeto drainage patterns occurring during a temporary inhibition of lava flow invasions in the valley. This unconformity, recognized for the first time in the periphery of the north-eastern flank of Etna by Branca and Catalano (2000), allowed us to separate the Ellittico volcano products from that of Mongibello. New $^{40}Ar/^{39}Ar$ age determinations define the time span during which Ellittico lava flows reached the floor of the paleo-Simeto valley in this sector of the volcano. The earliest recognized E1 lava flow, resting on the sedimentary terrains, has an isotopic age of 40.9±7.2 ka (BT sample). Following the emplacement of this lava flow, the paleo-

Table 3 Selected composition of glass measured in MB5 and MB17 scoria samples

	Sample																		
	MB5							MB17											
SiO_2	51.46	51.51	51.96	51.34	51.61	51.88	51.46	51.33	52.03	52.07	53.39	52.52	53.07	51.70	51.60	51.34	51.25	51.65	
TiO_2	2.31	2.24	2.31	2.36	2.36	2.39	2.31	2.39	2.35	2.11	2.09	2.25	2.32	2.39	2.35	2.16	2.32	2.33	
Al_2O_3	15.22	14.99	15.62	14.77	15.23	15.25	15.33	15.1	15.46	15.36	15.48	15.44	15.59	14.99	15.23	15.17	15.21	15.15	
FeO	11.09	10.99	10.67	11.32	11.23	11.1	11.53	11.1	10.86	11.07	10.74	10.37	10.91	10.65	10.77	11.24	10.96	11.59	
MnO	0.19	0.29	0.28	0.33	0.32	0.16	0.32	0.26	0.26	0.24	0.23	0.00	0.18	0.23	0.30	0.25	0.26	0.27	
MgO	2.73	2.82	2.81	2.87	2.94	2.99	2.97	2.84	2.93	2.61	2.63	2.54	2.44	3.14	2.95	3.12	3.32	3.13	
CaO	7.03	6.92	7.11	7.12	7.17	6.93	7.03	6.93	6.69	6.40	6.16	5.62	6.31	6.87	6.88	7.03	7.06	7.24	
Na_2O	3.68	3.65	3.97	3.41	3.36	3.51	3.55	3.52	3.52	3.93	4.19	4.34	3.68	3.61	3.77	3.30	3.24	2.92	
K_2O	2.83	2.92	2.98	2.95	2.87	2.89	2.99	2.8	2.94	3.25	3.25	3.22	3.16	2.91	2.87	2.84	2.65	2.80	
P_2O_5	1.04	0.93	0.93	0.98	0.9	1.01	1.06	0.94	0.99	0.87	0.82	0.91	0.83	1.00	0.96	1.02	0.94	0.94	
Total	97.98	97.62	98.96	97.83	98.39	98.45	98.91	97.60	98.22	97.92	98.97	97.21	98.47	97.49	97.68	97.47	97.21	98.02	

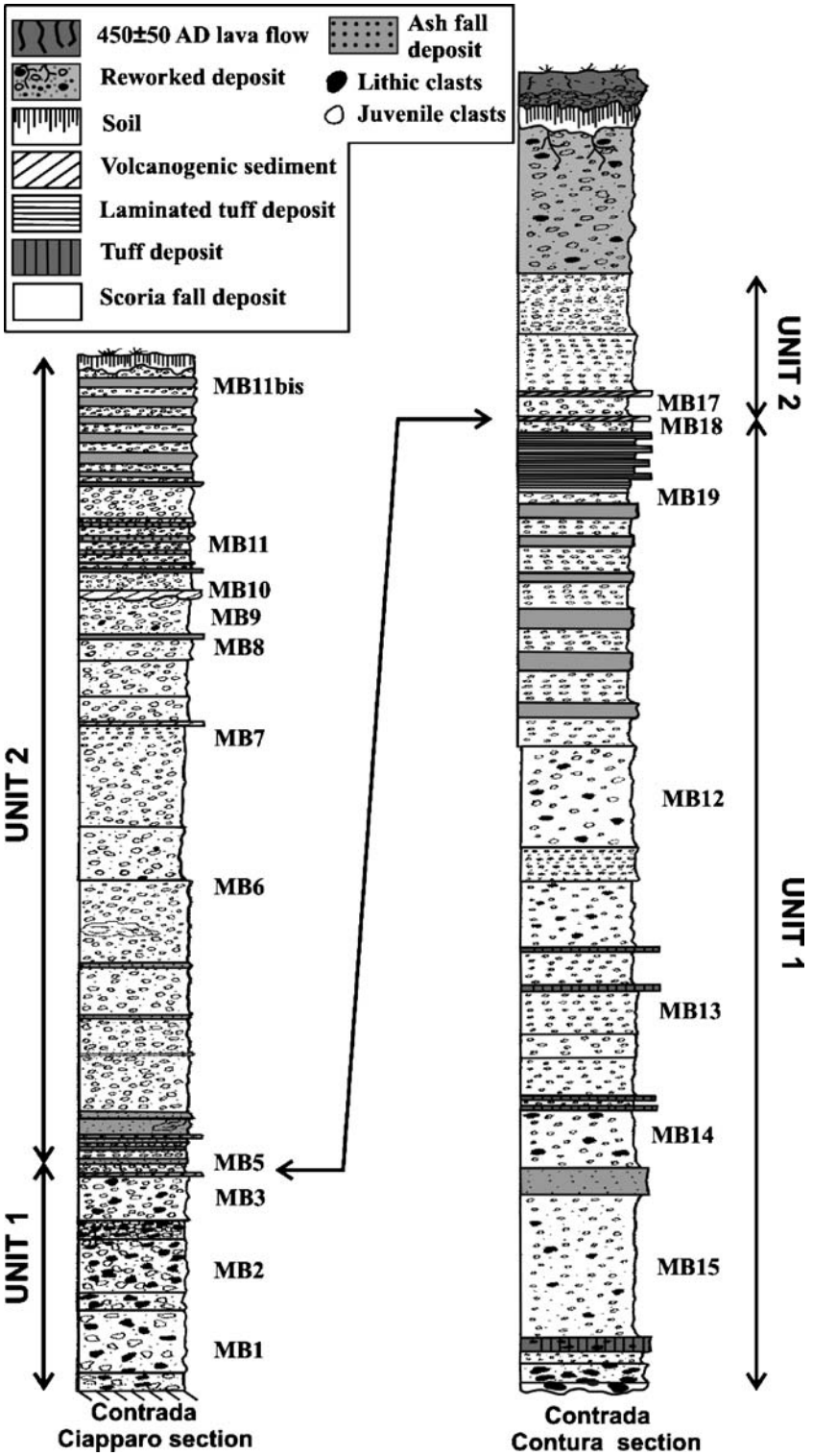

Fig. 10 Stratigraphic correlation between the Contrada Ciapparo and Contrada Contura sections

valley floor was invaded by other three lava flows (E2, E3, and E4). These lava flows are separated by both alluvial and lacustrine deposits, a few meters thick, as evidenced by subsurface data (Fig. 3) indicating periods during which the morphogenetic processes became predominant with respect to lava flow invasion. The new geochronological data of the BT sample are in agreement with the geological reconstruction of Branca et al. (2008) ruling out the presence of lava flows related to the earlier Na-alkaline volcanism (Ancient Alkaline Centers of Romano 1982) along the

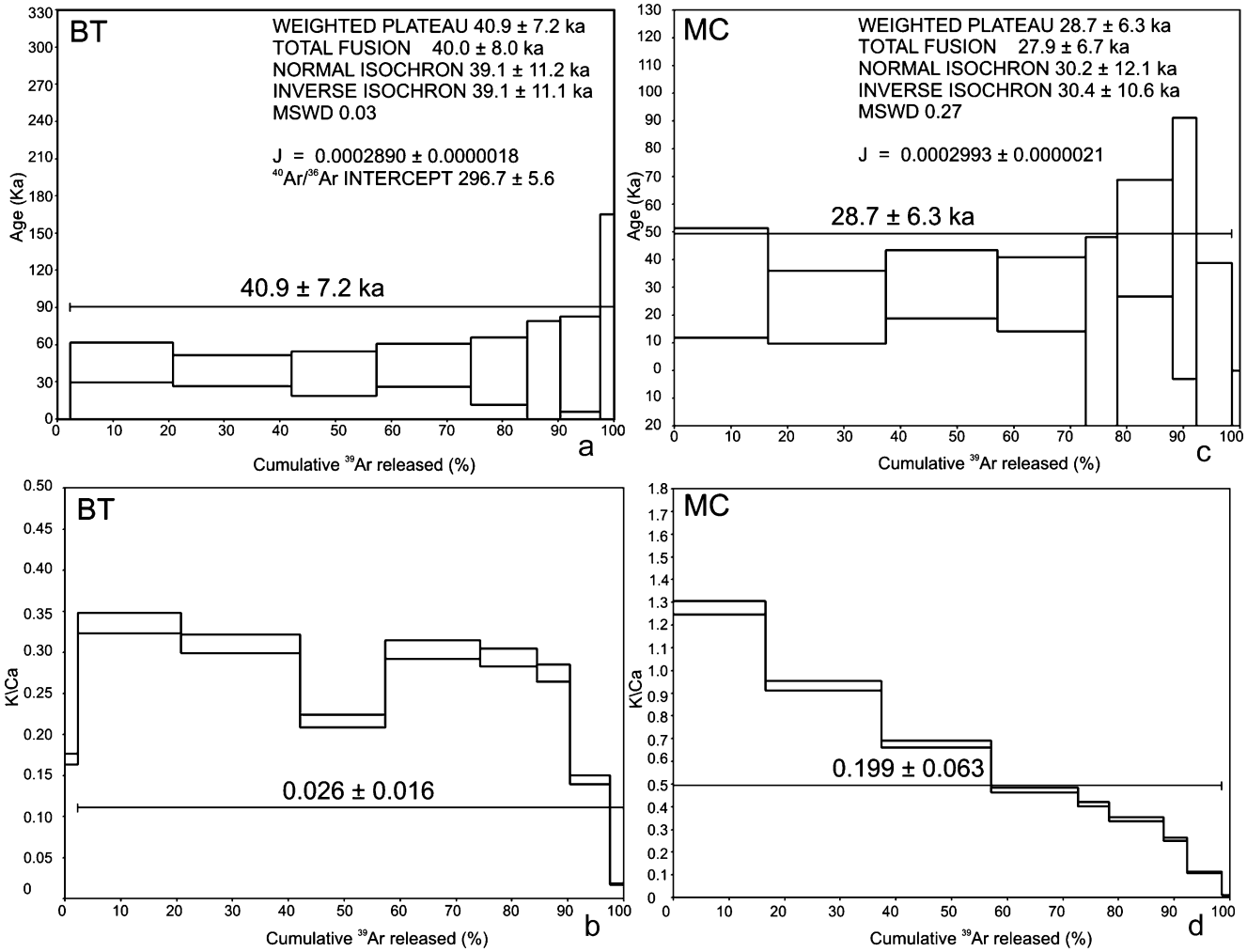

Fig. 11 Plateau age of **a** BT and **c** MC samples. Inside the diagram, there is additional information about weighted plateau age, total fusion age, normal and inverse isochron age, the value of MSWD, and the *J* value used to calculate the age and the isochron $^{40}Ar/^{36}Ar$ intercept. K/Ca diagram of **b** BT and **d** MC samples. In both diagrams, the *horizontal line* marks the used steps for the age calculation

valley floor of the Simeto River. Finally, the $^{40}Ar/^{39}Ar$ age obtained for the youngest Ellittico E5 lava flow (MC sample) indicates that the Mt Barca eruptive fissure formed 28.7±6.3 ka ago evidencing how this eruption did not occur during Mongibello volcano activity as previously inferred in the geological map of Romano et al. (1979) but during the activity of the Ellittico volcano.

The Mt Barca eruption started with explosive activity along the NE–SW-oriented eruptive fissure forming a spatter rampart. Thereafter, the main phase of activity continued in the upper part of the fissure where the scoria cone formed and tephra fallout deposited in the medial–distal areas. A short lava flow was emitted from the scoria cone base in the final stage of the eruption. The orientation of the preserved eruptive fissure corresponds to that of the extensional tectonic lineaments of the South Tyrrhenian system (Lentini et al. 2006) evidencing a control by the structural setting of the sedimentary basement on magma ascent in this peripheral sector of the volcano.

The Mt Barca explosive activity was characterized by two main phases, as suggested by the different types of deposits (Units 1 and 2) in its pyroclastic sequence (Fig. 10). The first phase formed a pyroclastic fall deposit made of high-density, poorly vesicular scoria lapilli and lithic clasts in variable percentage along the deposit, and a final thin stratified plane-parallel surge deposit (Unit 1), whereas the second phase produced typical strombolian fall deposits (Unit 2), composed by highly vesicular scoria lapilli beds interlayered with fine lapilli and ash beds. These layers can be related to periods of pause in the strombolian activity during which explosions occurring at the vent might have produced fine material that widely dispersed a few kilometers away. This phenomenon has been observed in some recent flank eruptions of Etna (e.g., 2001 see Taddeucci et al. 2004), lasting several weeks, during which the strombolian activity stopped for hours or days and was replaced by ash and gas venting or weak vulcanian-type activity. Dispersal of tephra fallout was toward the eastern sector of the volcano

since no deposits were found in the sedimentary terrains forming the right bank of the Simeto valley (Fig. 2). Conversely, the deposit presents a thickness of 2.35 m in the core located at a distance of about 2 km eastward from the vent. This inferred direction of the deposit dispersal corresponds to the main wind direction of the Etna region.

Petro-chemical analyses indicate that the magma erupted during the Mt Barca eruption is hawaiitic in composition as most of Etna volcanics (Corsaro and Pompilio 2004). Samples inside the deposits are homogeneous, showing no significant variation of the magma feeding the eruption. Stratigraphic correlation between the two sections has been done on the basis of the lithological features and physical parameters of the deposits. The lithic clasts in the lower part of the pyroclastic sequence reflect the stratigraphy of the country rock that the feeder dike encountered. The ratio between lava and sedimentary lithics varies from the base to the top, indicating that possible variations in the fragmentation level or collapse of the conduit system occurred during the eruption. In the lowermost samples, the dominant lithics are of E4 lava in both sections, suggesting the fragmentation level was in the lava flow cover. The upward increase of sedimentary lithics suggests a shifting of the fragmentation level toward the sedimentary substratum. The sudden variation of juvenile clast density indicates variations in the condition of magma fragmentation. High-density value for the basal samples MB1, MB2, and MB3 in Contrada Ciapparo and from MB15 to MB12 may reflect magma–water interaction that prevented gas bubble expansion. The high density of these samples of Unit 1 are those typical of phreatomagmatic processes (Houghton and Wilson 1989) in contrast with low density values of the clasts of Unit 2 evidencing a purely magmatic phase in the second part of the eruption.

After the Mt Barca eruption, a period of erosion affected the lower NW flank of the volcano. In particular, the entrenchment of the paleo-Simeto main drainage axis carved the Ellittico lava flow succession that presently form a terraced body along the left bank of the Simeto River. At the same time, the modification of the drainage network produced an alluvial deposit that partially covered the Ellittico lava flows. The age of about 20 ka assigned to this alluvial deposit by Chester and Duncan (1982) is in agreement with our stratigraphic setting and the reconstructed geological evolution of the investigated area. Finally, during the eruptive activity of the past 15 ka, only four lava flows reached the upper Simeto Valley and three of them occurred in historical time.

Conclusion

Geological data of the lower north-western flank of Etna together with $^{40}Ar/^{39}Ar$ age determinations have enabled us to detail the evolution of this peripheral area of the volcano corresponding to the upper Simeto River valley. This sector of the volcano was subjected to lava flow invasion during Ellittico volcano activity since 40.9±7.2 ka ago. In this period, four lava flows reached the valley floor, damming the main drainage axis several times. The youngest Ellittico products of this area are related to a peripheral magma intrusion occurring 28.7±6.3 ka ago forming the Mt Barca eruptive fissure located close to the valley floor between 580 and 700 m of altitude. Following this eruption, the upper Simeto valley was involved in erosional processes that caused the entrenchment of the main drainage axis producing an alluvial terrace deposit on the Ellittico lava flows. This erosional phase corresponds to a main unconformity recognized on the peripheral sectors of Etna edifice separating Ellittico volcano products from those of Mongibello volcano.

Tephrostratigrafic study of Mt Barca deposits allowed defining the eruptive style of this flank eruption occurring 15 km away from the summit craters whose magma intrusion was driven by the tectonic structures of the sedimentary basement. This flank eruption was characterized mainly by an intense explosive activity and minor effusion generating a 1.1-km-long lava flow. The explosive activity formed Mt Barca scoria cone at 700 m elevation, a spatter rampart NE–SW-oriented and several-meter-thick scoria fall deposits dispersed eastward. Field and analytical data allow two eruption phases to be defined. The rising feeder dike cut the Numidian Flysch and the E4 lava flow interacting with shallow groundwater hosted between the impermeable sedimentary basement and the overlying E4 lava flow. The first phase was characterized by a magma–water interaction producing phreatomagmatic explosions (Unit 1); conversely, the second phase was purely magmatic-forming strombolian deposits (Unit 2).

This eruptive behavior, characterized by intense and complex explosive activity, has already been documented in the case of the Contrada Ragaglia eruption that occurred 18.7 ka in the lower north-eastern flank of Etna at about 500 m elevation (Andronico et al. 2001). We note that the geological and structural setting of the peripheral sectors of the volcanic edifice can favor the recurrence of flank eruptions characterized by vigorous explosive activity as a consequence of the interaction between the rising magma and the shallow groundwater hosted in the volcanic pile. Therefore, the occurrence in pre-historical times of this type of flank eruptions indicates that the highly explosive eruptive events occurring in the upper flanks of the volcano during the past three centuries (Branca and Del Carlo 2005) may also affect the lower ones close to the highly densely inhabited area. In terms of hazard assessment, even though the lava effusion represents the main type of volcanic hazard for the inhabited area, the possible occurrence of

highly explosive flank eruptions widens the expected eruption scenarios at Mt Etna.

Acknowledgments We are very grateful to L. Miraglia from the Istituto Nazionale di Geofisica e Vulcanologia, Sezione di Catania for assistance with SEM–EDS instrument and to K. de Groote, M. Groen, and B.S.H. Schneider for their support to the isotopic measurements at the Argon laboratory of the Vrije Universiteit. We wish to thank Cioni R., Duncan A.M., and Keating G. for their helpful reviews and suggestions. The research was financially supported by INGV-DPC V3_6 project UR V3_6/07 (Resp. M. Coltelli).

Appendix

$^{40}Ar/^{39}Ar$ methodological approach

To chronologically constrain the geological evolution of the studied area, we selected two lava flow samples. The first one was collected from E1 lava flow along the left bank of the Simeto River (BT sample in Fig. 2). This lava flow is the oldest unit recognized in the studied area and was attributed to the earlier Na-alkaline volcanism (Ancient Alkaline Centers unit of Romano 1982) in the geological map of Romano et al. (1979). The second sample (MC sample in Fig. 2) belonging to the E5 lava flow was collected with the aim of defining the age of the Mt Barca eruption.

After removal of weathered portions, samples were crushed to obtain a grain-size fraction between 250 and 500 μm. The phenocryst fractions plagioclase, olivine, and pyroxenes were removed by density separation using heavy liquid at 27 and 29×10^2 kg/m^3. A final clean separate was obtained after acid leaching with dilute HNO_3 and HF followed by hand picking for any obvious phenocryst intergrowths left in the sample. Samples were wrapped in Al foil and loaded into a quartz tube together with standards (DRA sanidine of 25.26±0.05 Ma) for irradiation (duration: 1 h) with fast neutrons in the Cd-lined RODEO facility of the EU-JRC Petten HFR reactor (Netherlands). After irradiation, ca. 50% of the sample (ca. 200 mg) was wrapped in Al foil and loaded into a 21-position sample carousel in a double vacuum high temperature furnace. Gas extraction, purification, and mass spectrometric measurement follow the procedures described in Schneider et al. (2007). In summary, gas was extracted in steps of increasing furnace temperature between ca. 700°C and 1,200°C. The furnace segment of the extraction system is fitted with a cold trap that is used to trap any volatile components coming off the sample during heating. After cooling of the furnace tube, the gas is expanded into the purification line where it is exposed to two or three stages of cleaning by exposure to activated Fe–V–Zr and Zr–Al alloys at temperatures of 250°C and 450°C, respectively. Finally, the purified argon gas is admitted into the mass spectrometer for isotopic analysis. In this system, we use a Hiden HAL IV RC PIC-RGA 101 instrument fitted with a dual filament open electron bombardment source and a dual Faraday channeltron collector. The channeltron collector is operated in pulse-counting mode. Peak shapes are predictable with flat tops of better then ca. 0.4 *m*/*e* (mass over charge), and full separation of peaks (peak valleys in the parts per million range). Typically, beam intensities are measured at seven positions on the peak top from *m*/*e* −0.1 to *m*/*e* +0.2 for masses 36, 39, and 40, and single positions for masses 37 and 38. One baseline is measured at *m*/*e* 35.45. Intensity data are averaged per peak, and intensity information with the respective standard deviations are regressed in ArArCalc2.40 (Koppers 2002 and http://www.earthref.org/tools/ararcalc.htm). Beam intensities are corrected for hot and cold line blanks, intensity-dependent mass discrimination, and radioactive decay during the time interval between irradiation and analysis. Subsequently, we follow a standard intensity de-convolution scheme to correct for nucliogenic ^{36}Ar, ^{39}Ar, and ^{40}Ar using production rates measured from pure K and Ca silicate glass. Cold blanks were in the range 45, 5, 11, 20, and 14,000 cps at *m*/*e*: 36, 37, 38, 39, and 40, respectively, whereas the hot blanks varied from indistinguishable from the cold blank at 700°C to 55, 5, 17, 20, and 16,000 cps at 1,000°C and 130, 12, 27, 16, and 34,000 cps at 1,200°C.

References

Andronico D, Branca S, Del Carlo P (2001) The 18.7 ka phreatomagmatic flank eruption on Etna (Italy): relationship between eruptive activity and sedimentary basement setting. Terra Nova 13(4):235–240

Andronico D, Branca S, Calvari S, Burton MR, Caltabiano T, Corsaro RA, Del Carlo P, Garfì G, Lodato L, Miraglia L, Muré F, Neri M, Pecora E, Pompilio M, Salerno G, Spampinato L (2005) A multidisciplinary study of the 2002–03 Etna eruption: insights for a complex plumbing system. Bull Volcanol 67(4):314–330

Ben Avraham Z, Grasso M (1990) Collisional zone segmentation in Sicily and surrounding areas in the central Mediterranean. Ann Tecton 4:131–139

Branca S (2003) Geological and geomorphologic evolution of the Etna volcano NE flank and relationships between lava flow invasions and erosional processes in the Alcantara Valley (Italy). Geomorphology 53:247–261

Branca S, Catalano S (2000) Stratigraphical and morphological criteria for the reconstruction of UBSU in the peripheral area of Mt. Etna (Italy). Mem Soc Geol Ital 55:181–187

Branca S, Del Carlo P (2005) Types of eruptions of Etna Volcano AD 1670–2003: implications for short-term eruptive behaviour. Bull Volcanol 67:732–742

Branca S, Ferrara V (2001) An example of river pattern evolution produced during the lateral growth of a central polygenic volcano: the case of the Alcantara river system, Mt Etna (Italy). Catena 45/2:85–102

Branca S, Coltelli M, Groppelli G (2004a) Geological evolution of Etna volcano. In: Bonaccorso A, Calvari S, Coltelli M, Del Negro C, Falsaperla S (ed) Mt Etna Volcano Laboratory. AGU (Geophysical monograph series) 143, pp 49–63

Branca S, Coltelli M, Del Carlo P, Groppelli G, Norini G, Pasquaré G (2004b) Stratigraphical approaches and tools in the geological mapping of Mt. Etna volcano. In: Pasquarè G, Venturini C (eds) Mapping geology in Italy. APAT-Dipartimento Difesa del Suolo, Servizio Geologico d'Italia, S.EL.CA, Firenze, pp 145–156

Branca S, Coltelli M, De Beni E, Wijbrans J (2008) Geological evolution of Mount Etna volcano (Italy) from earliest products until the first central volcanism (between 500 and 100 ka ago) inferred from geochronological and stratigraphic data. Int J Earth Sci 97:135–152, DOI 10.1007/s00531-006-0152-0

Chester DK, Duncan AM (1979) Interrelationships between volcanic and alluvial sequences in the evolution of the Simeto River Valley, Mount Etna, Sicily. Catena 6:293–315

Chester DK, Duncan AM (1982) The interaction of volcano activity in Quaternary times upon the evolution of the Alcantara and Simeto rivers, Mount Etna, Sicily. Catena 9:319–342

Chester DK, Duncan AM, Guest JE, Kilburn CRJ (1985) Mount Etna: the anatomy of a volcano. Chapman and Hall, London

Coltelli M, Del Carlo P, Vezzoli L (2000) Stratigraphic constrains for the explosive activity in the last 100 ka at Etna volcano, Italy. Int J Earth Sci 89:665–677

Corsaro RA, Pompilio M (2004) Dynamics of magmas at Mount Etna. In: Bonaccorso A, Calvari S, Coltelli M, Del Negro C, Falsaperla S (ed) Mt Etna Volcano Laboratory. AGU (Geophysical monograph series) 143, 91–110

De Beni E, Wijbrans JR, Branca S, Coltelli M, Groppelli G (2005) New results of $^{40}Ar/^{39}Ar$ dating constrain the timing of transition from fissure-type to central volcanism at Mount Etna (Italy). Terra Nova 17(3):292–298

Dunai TJ, Wijbrans JR (2000) Long-term cosmogenic 3He production rates (152 ka–1.35 Ma) from $^{40}Ar/^{39}Ar$ dated basalt flows at 29° N latitude. Earth Planet Sci Lett 176:147–156

Houghton BF, Wilson CJN (1989) A vesicularity index for pyroclastic deposits. Bull Volcanol 51:451–462

Koppers AAP (2002) ArArCALC-software for $^{40}Ar/^{39}Ar$ age calculations. Computers and Geosciences 28:605–619

Jarosewich E, Nelen JA, Norberg JA (1980) Reference samples for electron microprobe analysis. Geostand Newsl 4(1):43–47

Le Maitre RW (ed.) (1989) A classification of igneous rocks and glossary of terms. Blackwell Scient Publ, Oxford

Lentini F (1982) The geology of the Mt. Etna basement. Mem Soc Geol Ital 23:7–25

Lentini F, Carbone S, Guarnieri P (2006) Collisional and postcollisional tectonics of the Apenninic-Maghrebian orogen (southern Italy). In Dilek Y and Pavlides S (eds) Postcollisional tectonics and magmatism in the Mediterranean region and Asia. GSA Special Paper 409, pp 57–81

McGuire WJ, Pullen AD (1989) Location and orientation of eruptive fissures and feeder-dykes at Mount Etna: influence of gravitational and regional tectonic stress regimes. J Volcanol Geotherm Res 38:352–344

Rowland SK, Walker GPL (1987) Toothpaste lava: characteristics and origin of a lava structural type transitional between pahoehoe and aa. Bull Volcanol 49:631–641

Romano R (1982) Succession of the volcanic activity in the Etnean area. Mem Soc Geol Ital 23:27–48

Romano R, Lentini F, Sturiale C et alii (1979) Carta Geologica del Monte Etna Scala 1:50.000. In: Mem Soc Geol It 23

Salvador A (1987) Uncorformity-bounded stratigraphic units. Geol Soc Am Bull 98:232–237

Salvador A (1994) International stratigraphic guide, GSA Salvador A (ed), Boulder, 1–214

Scollo S, Del Carlo P, Coltelli M (2007) Tephra fallout of 2001 Etna flank eruption: analysis of the deposit and plume dispersion. J Volcanol Geotherm Res 160:147–164

Sturiale C (1967) Le vulcaniti rinvenute in un pozzo trivellato presso Bronte (Etna). Atti Accad Gioenia Sci Nat XIX:93–109

Schneider BSH, Kuiper KF, Postma O, Wijbrans JR (2007) A furnace extraction system for $^{40}Ar/^{39}Ar$ geochronology of young basalts. EGU General Assembly 2007, EGU2007-A-10055

Taddeucci J, Pompilio M, Scarlato P (2004) Conduit processes during the July–August 2001 explosive activity of Mt. Etna (Italy): inferences from glass chemistry and crystal size distribution of ash particles. J Volcanol Geotherm Res 137:33–54

Tanguy JC, Condomines M, Le Goff M, Chillemi V, La Delfa S, Patanè G (2007) Mount Etna eruptions of the last 2,750 years: revised chronology and location through archeomagnetic and $^{226}Ra–^{230}Th$ dating. Bull Volcanol 70:55–83

Walker GPL (1973) Explosive volcanic eruptions, a new classification scheme. Geol Rundsch 62:431–446